Acta Pharmaceutica Sinica B 2025;15(4):1991−2007

Chinese Pharmaceutical Association
Institute of Materia Medica, Chinese Academy of Medical Sciences

Acta Pharmaceutica Sinica B

www.elsevier.com/locate/apsb
www.sciencedirect.com

ORIGINAL ARTICLE

SAE1 promotes tumor cell malignancy *via* SUMOylation and liquid−liquid phase separation facilitated nuclear export of p27

Ling Wang[a,b,†], Jie Min[b,†], Jinjun Qian[b,†], Xiaofang Huang[d,†], Xichao Yu[b], Yuhao Cao[b], Shanliang Sun[c], Mengying Ke[b], Xinyu Lv[b], Wenfeng Su[a], Mengjie Guo[b], Nianguang Li[c], Shiqian Qi[d,*], Hongming Huang[a,*], Chunyan Gu[b,*], Ye Yang[a,b,*]

[a]*Department of Hematology, Affiliated Hospital of Nantong University, Nantong 226001, China*
[b]*School of Medicine, Nanjing University of Chinese Medicine, Nanjing 210023, China*
[c]*School of Pharmacy, Nanjing University of Chinese Medicine, Nanjing 210023, China*
[d]*Department of Urology, Institute of Urology, State Key Laboratory of Biotherapy, West China Hospital, College of Life Sciences, Sichuan University, and National Collaborative Innovation Center, Chengdu 610041, China*

Received 21 August 2024; received in revised form 29 November 2024; accepted 20 December 2024

KEY WORDS

Cancer;
Multiple myeloma;
Post-translational modifications;
SAE1;
SUMOylation;
p27;
Liquid−liquid phase separation;
Colchicine

Abstract Most cancers are currently incurable, partly due to abnormal post-translational modifications (PTMs). In this study, we initially used multiple myeloma (MM) as a working model and found that SUMOylation activating enzyme subunit 1 (SAE1) promotes the malignancy of MM. Through proteome microarray analysis, SAE1 was identified as a potential target for bioactive colcemid or its derivative colchicine. Elevated levels of SAE1 were associated with poor clinical survival and increased MM proliferation *in vitro* and *in vivo*. Additionally, SAE1 directly SUMOylated and upregulated the total protein expression of p27, leading to LLPS-mediated nuclear export of p27. Our study also demonstrated the involvement of SAE1 in other types of cancer cells, and provided the first monomer crystal structure of SAE1 and its key binding model with colchicine. Colchicine also showed promising results in the Patient-Derived Tumor Xenograft (PDX) model. Furthermore, a controlled clinical trial with 56 MM patients demonstrated the clinical efficacy of colchicine. Our findings reveal a novel mechanism by which

*Corresponding authors.
E-mail addresses: yangye876@sina.com, 290422@njucm.edu.cn (Ye Yang), guchuanyan@njucm.edu.cn (Chunyan Gu), hhmmmc@163.com (Hongming Huang), qishiqian@scu.edu.cn (Shiqian Qi).
[†]These authors made equal contributions to this work.
Peer review under the responsibility of Chinese Pharmaceutical Association and Institute of Materia Medica, Chinese Academy of Medical Sciences.

https://doi.org/10.1016/j.apsb.2025.02.011

tumor cells evade p27-induced cellular growth arrest through p27 SUMOylation-mediated nuclear export. SAE1 may serve as a promising therapeutic target, and colchicine may be a potential treatment option for multiple types of cancer in clinical settings.

1. Introduction

Although significant progress has been made in the development of new drugs and treatment strategies for cancer, most cancers are still incurable. To address this issue, we focus on multiple myeloma (MM), the second most common hematologic malignancy, as a model for exploring novel therapeutic targets and drugs. The majority of MM patients eventually relapse due to the clonal expansion of abnormal plasma cells and the massive production of antibodies, which require a delicate balance of protein homeostasis and post-translational regulation[1]. Post-translational modifications (PTMs), such as phosphorylation, acetylation, and ubiquitination, play a crucial role in the occurrence and development of various cancers, including MM[2,3]. Several first-line drugs, including bortezomib (BTZ) approved for MM patients, target key factors in the protein PTM pathway[2]. However, there is a lack of research on the small ubiquitin-like modifier (SUMO) PTM in MM, making it a promising area for the development of PTM-centered therapeutics and identification of novel targets.

SUMOylation, the process of modifying proteins with SUMO, has been shown to impact cell cycle, growth, metastasis, and apoptosis by regulating subcellular localization, function, and interaction of proteins[4]. Similar to the enzymatic E1−E2−E3 cascade in ubiquitination, SUMOylation involves the covalent attachment of SUMO (∼12 kDa) to Lys residues of substrates in a sequential reaction of SUMO processing and transferring. The initiation of this process is carried out by the SUMO1-activating enzyme subunit 1 (SAE1), which forms an ATP-dependent thioester bond between the mature SUMO protein and SAE2/UBA2, leading to subsequent conjugation, activation, and ligation in the SUMO protein modification processes[5]. Previous studies have identified SAE1 as a potential biomarker for disease progression and prognosis in glioma, hepatocellular carcinoma, and triple-negative breast cancer[6,7]. Over-activated SUMOylation pathway, involving the SUMO-conjugating E2 Ubc9 and SUMO-E3 PIAS1 in MM bone marrow is associated with adverse clinical outcomes compared to healthy individuals[8,9]. Therefore, targeting the SAE1-mediated SUMOylation pathway may be a promising strategy to develop therapeutics for both blood and solid tumors.

Natural products and synthetic derivatives contribute to nearly 50% or more of the FDA-approved (antitumor) drugs[10]. The groundbreaking research conducted by Zhang et al. has shown that arsenic trioxide (ATO), a notoriously toxic substance, can effectively treat acute promyelocytic leukemia (APL) and turn it into a rare but curable malignancy[11,12]. Based on the "like cures like" concept, our research group also utilized ATO as a probe and identified a drug target, glycinamide ribonucleotide transformylase (GART), which functions as a novel methyltransferase to promote tumor stemness in colorectal cancer[13]. Additionally, we used the traditional Chinese medicine bioactive molecule Bufalin as a probe and discovered that AHSA1 (activator of HSP90 ATPase activity 1) is a promising therapeutic target for cellular proliferation and resistance to proteasome inhibitors, such as BTZ in MM[14]. The current study focuses on the alkaloids extracted from the lily plant *Colchicum* sp., specifically colchicine, and its derivative colcemid (or demecolcine) for the following reasons: Firstly, colchicine has been used as a drug for over 200 years due to its anti-inflammatory and anticancer properties, such as treating gout (FDA approved in 2009), FMF (familial Mediterranean fever), amyloidosis, cirrhosis, and psoriasis[15]. Secondly, in addition to their effectiveness in binding and inhibiting tubulin polymerization, colchicine has also been found to be effective against lung cancer cells at a less toxic dose, and colcemid has been used for treating myelocytic leukemia and malignant lymphoma[16,17]. Therefore, it would be of great value to further discover and develop possible therapeutic targets of colchicine/colcemid and their downstream working mechanisms.

In this study, we first confirmed the antitumor effects of colchicine/colcemid in MM and utilized human proteomic microarrays with Cy5-labeled colcemid probes to screen for and investigate the function of SAE1, a potential novel target of colchicine/colcemid. We also elucidated the pro-oncogenic mechanism by which SAE1 could increase the expression of p27, a classic tumor suppressor for cell proliferation, but facilitate the nuclear export of p27 *via* SUMOylation mediated liquid−liquid phase separation (LLPS) during tumor cell malignancy. Furthermore, we extended our investigation to examine the relationship between SAE1 expression, colchicine, and pathological characteristics in various blood and solid cancers. At the clinical level, we evaluated the effectiveness of colchicine in treating MM patients who had previously been treated with and developed resistance to BTZ or Lenalidomide. Our discovery of SAE1 as a promising therapeutic target may pave the way for the clinical use and development of colchicine as an effective strategy for multiple types of cancers.

2. Materials and methods

2.1. Gene expression profiling

Gene expression profiles of patients with MM were obtained from the analysis of cohorts of patients with total treatment 2 (TT2) and proteasome inhibition prolonged remission (APEX), which are available from the GEO database as previously described[18].

2.2. Antibodies and reagents

The primary antibodies used in this study were as follows: SAE1 (13585 S, Cell Signaling Technology, USA; MA530835, ThermoFisher Scientific, USA); SUMO1 (10329-1-AP, ProteinTech Group, China); p27 (3686 S, Cell Signaling Technology, USA; 25614-1-AP, ProteinTech Group, China); β-actin (4970 S, Cell Signaling Technology, USA); ubiquitin (10201-2-AP,

ProteinTech Group, China); HA (51064-2-AP, ProteinTech Group, China); CDK6 (14052-1-AP, ProteinTech Group, China); CDK4 (11026-1-AP, ProteinTech Group, China); CyclinD1 (55506 T, Cell Signaling Technology, USA); Histone-H3 (17168-1-AP, ProteinTech Group, China); 6x-his (66005-1-Ig, ProteinTech Group, China); GAPDH (66004-1-Ig, ProteinTech Group, China); GST (66001-2-Ig, ProteinTech Group, China); anti-DYKDDDDK (101274-mm05t, Sino Biological, China); CRM1 (sc-74454, Santa Cruz, USA). The second antibodies goat anti-rabbit IgG(H + L) HRP (FMS-Rb01, Fcmacs); goat anti-mouse IgG(H + L) HRP (S0002, Affinity, USA); goat pab to mouse IgG (FITC) (ab6785, Abcam, UK); goat anti-rabbit IgG (H + L) Fluor647-conjugated (S0013, Affinity, USA). Doxycycline (DOX) and rabbit IgG (a7016) were purchased from the Beyotime (Shanghai, China). Puromycin was obtained from Merck KGaA (Darmstadt, Germany). Cell Counting Kit-8 (CCK-8) was purchased from Apexbio (Houston, USA). Colcemid and Colchicine (COL) were purchased from Fusheng Industry (Shanghai, China). Bortezomib (BTZ) was purchased from Selleck Chemicals (Houston, TX).

2.3. Cell lines and cell culture

Human MM cell lines ARP1 and H929 and human acute myeloid leukemia cell line MOML-13 were cultured in RPMI1640. HEK293, human lung cancer cell line A549, human liver cancer cell line HepG2, and human colon cancer cell line RKO were cultured in DMEM (ThermoFisher Science, USA). 10% fetal bovine serum (American Gibco), penicillin (100 U/mL, HyClone USA), and streptomycin (100 μg/mL, HyClone, USA) were added to the culture medium and replaced every 2 days. All cells were cultured in 100 mm dishes at 37 °C in a 5% CO_2 incubator.

2.4. Plasmids and cell transfection

Plasmids containing human SAE1 cDNA and SAE1 shRNA were provided by TranSheepBio (Shanghai, China). The cDNA sequence of SAE1 was cloned into a PTSB vector with GFP fluorescence and Flag tag, and SAE1-targeting shRNA was inserted into the pTRIPZ vector, which was controlled by DOX-inducible promoter. The expression vector (SAE1 cDNA/SAE1 shRNA) and packaging vector (PLP1, PLP2, VSVG) were co-transferred into HEK293 cells by Lipofectamine transfection reagent (YEASEN, Shanghai). After 48 h, the virus supernatant was collected, concentrated, and stored at −80 °C. Puromycin was used to screen the lentivirus transfection efficiency in cell lines.

2.5. Cell proliferation, cell cycle, and apoptosis assays

Cell Counting Kit-8 (CCK-8) was used to detect cell proliferation and cell viability at 24, 48, and 72 h in 96-well plates respectively. The absorbance at 450 nm was measured to calculate the number of viable cells. In soft agar clone formation experiments, clone growth was measured by mixing 1×10^4 cells well in a 1 mL mixture of 3.3% agar/RPMI1640 + 10% FBS +1% PS. The culture medium was replenished twice a week and cells were cultured for 3−4 weeks. If the number of cells was >40, they were considered to be clone-forming colonies. The colonies were imaged and the number of colonies was counted using ImageJ. Flow cytometry (Merck, Darmstadt, Germany) and the BrdU APC Flow Kit (UNIV, China) were applied to detect cell cycle and apoptosis as described above.

2.6. Co-immunoprecipitation (Co-IP)

In accordance with the manufacturer's instructions, a Pierce Direct Magnetic IP/CO Immunoprecipitation (Co-IP) Kit (ThermoScientific) was used for the Co-IP assay. Primary antibodies for SAE1 and SUMO1 were used to enrich the corresponding proteins in ARP1 WT and ARP1 SAE1-OE cells. We diluted the antibodies and incubated them with the beads overnight on a spinning machine at 4 °C. The next day, more than 10 million cells from each cell line were lysed, added to the processed beads, and incubated overnight. On the third day, the specific protein bound to the beads was eluted, followed by the WB analysis and the Mass spectrometry (MS) analysis.

2.7. Recombinant plasmid construction

Plasmid primers and digestion sites are shown in Supporting Information Table S1. PCR was performed with a Phanta Super-Fidelity DNA Polymerase kit (Vazyme, Nanjing). Gel recovery was made with the Agarose Gel Recovery Kit from Tiangen Biochemical Co. The overlapping PCR reactions were also performed using the Phanta Super-Fidelity DNA Polymerase kit (Vazyme, Nanjing, China). The procedure for touch down PCR reaction was: pre-denaturation at 94 °C for 5 min, denaturation at 94 °C for 30 s, annealing at 70 °C for 2 cycles → 68 °C for 2 cycles → 66 °C for 2 cycles → 64 °C for 2 cycles → 62 °C for 25 cycles.

2.8. Mass spectrometry (MS) analysis

SDS-PAGE was applied to separate proteins, and gel bands were excised and digested with sequencing-grade trypsin (Promega, USA). The peptides obtained were analyzed using a Q exactive mass spectrometer (ThermoFisher Scientific). Fragment spectra were analyzed against the National Center for Biotechnology Information's Non-Redundant Protein Database.

2.9. Liquid chromatograph−mass spectrometry (LC−MS) analysis

The purified SAE1 protein was incubated with colcemid at 4 °C for 24 h. The analysis process was performed through waters QTOF, and the data were deconvoluted by UNIFI software. After desalting and tryptic digestion, PEAKS software was used to analyze data for binding site ID.

2.10. Small molecule-SAE1 binding mode prediction

The crystal structures of SAE1 (PDB: 8VY5) were retrieved from pdb bank (https://www.pdbus.org/) and were prepared by Schrödinger[19] software using "protein preparation" with default settings. Subsequently, to predict the potential binding site of colchamine/colchicine, we performed site prediction based on crystal structures using the Sitemap tool[20,21] of Schrödinger. Based on each predicted binding site, corresponding grid files were generated. Small molecule (in SMILES format) preparation calculations were performed by Schrödinger's LigPre panel, including adding hydrogens, generating possible conformations as well as protonation. Molecular docking was performed by Glide[22] using the "extra precision (XP)" mode and generated 30 poses for each ligand.

2.11. Microscale thermophoresis (MST)

Purified protein SAE1 at a concentration of 10 μmol/L was fluorescently labeled with the Monolith™ RED-NHS second generation protein labeling kit (NanoTemper Germany). Different drug concentrations were set and the different drug concentrations were mixed thoroughly with the same concentration of SAE1 protein, and incubated for 5 min at room temperature, the mixture was aspirated with a capillary tube and tested for binding capacity using a new generation biomolecular interaction assay (NanoTemper Germany). The K_d values were calculated by analytical software.

2.12. Isothermal Titration Calorimetry (ITC)

Continuously and accurately monitoring and recording the calorimetric curve of a changing process were conducted through highly sensitive and automated microcalorimetry. The K_d values were calculated by analytical software.

2.13. Immunofluorescent staining and confocal microscopy

IF staining was as previously described[23]. A confocal microscope (TCS SP8, Leica, Germany) was used to capture images.

2.14. Immunohistochemistry analysis (IHC)

Immunostaining was carried out on paraffin tissue sections. The main procedure involved was as follows: the samples on the slides were incubated with the primary antibody at 4 °C overnight. Subsequently, the secondary antibody was applied and held at 37 °C for 45 min, followed by drops of SABC at 37 °C for 30 min. The samples were stained brown with DAB solution and finally counterstained with hematoxylin for light color.

2.15. Nuclear paddle protein isolation assay

We used the Beyotime Nucleoprotein and Cytoplasmic Protein Extraction Kit (Shanghai, China) to extract nucleoproteins and paddle proteins and performed the experiments according to the manufacturer's instructions. A total of 15−30 μg of protein per cell was separated on a 15% SDS-PAGE gel and then transferred to a PVDF membrane. After blocking with 5% skimmed milk, proteins were detected with the appropriate antibodies.

2.16. In vitro droplet assay

For protein purification, plasmids containing the GFP fusion protein were transformed into BL21 cells, and a fresh bacterial colony with an OD_{600} of 0.6 was induced with 1 mmol/L IPTG at 20 °C overnight. The residue was collected by centrifugation, diluted with Buffer A solution (pH = 7.5, 500 mmol/L NaCl, 500 mmol/L HEPES, 5 mmol/L imidazole, 5% glycerol), protease inhibitor added, and homogenized at 900 V for 15 min. The supernatant was collected by breaking the residue and filtered through a 0.45 μm aqueous membrane. The protein with His tag was bound to a nickel ion affinity column and the target protein was obtained by gradient elution with Buffer B (pH = 7.5, 500 mmol/L NaCl, 500 mmol/L HEPES, 500 mmol/L imidazole) with the aid of an AKTA protein separation and purification platform (AKTA pure L, Cytiva, USA). Purity was then determined by coomassie-stained gels, followed by protein concentration by GF Buffer (pH = 8, 50 mmol/L Nacl, 20 mmol/L Tris). For the droplet assay, proteins were diluted to different concentrations, and GF Buffer (pH = 8, 50 mmol/L NaCl, 20 mmol/L Tris) was added to different concentrations of proteins. Immediately after induction of the protein solution with 10% PEG8000, a uniform drop was added to a confocal dish, and imaging was obtained through a Leica TCS SP8 confocal microscope (TCS SP8, Leica, Germany).

2.17. Fluorescence recovery after photobleaching (FRAP)

HEK293 cells transfected with p27 or p27-DM plasmid were subjected to FRAP experiments with a confocal microscope (TCS SP8, Leica, Germany). Photobleaching was performed using tornado mode with a 488 nm laser at 80% laser power. GFP fluorescence recovery was monitored with a 488 nm laser using the free-run mode at ∼5 s intervals. Fluorescence of unbleached sites in the same view was also monitored as the control. The signal was presented as the ratio relative to the fluorescence signal before photobleaching.

2.18. GST pull-down assays

The GST pull-down assay was performed using the Pierce GST Protein Interaction Pull-down Kit (Thermo Scientific, 21516) according to the manufacturer's recommendations. GST-pEGX-4T-1-SAE1 and PET28A-His-p27 were transformed into *E. coli* BL21. Bacterial colonies were induced with 1 mmol/L IPTG overnight at 20 °C, and lysates were collected. Bacterial lysates containing GST-SAE1 were incubated with glutathione agarose overnight at 4 °C and washed. Bacterial lysates containing His-p27 were eluted from the beads with GST-SAE1 and bound proteins using 10 mmol/L glutathione elution buffer and subjected to gel analysis.

2.19. In vitro SUMOylation assay

His-tagged SAE1, p27, p27-DM, and SAE1-E74 proteins were expressed and purified by *E. coli* BL21. For *in vitro* SUMOylation assays, the SUMOylation assay kit (ab139470) was purchased from Abcam according to the manufacturer's protocol. Briefly, the regulator and purified protein were mixed as indicated and incubated at a constant temperature of 37 °C for 1 h, followed by the addition of 20 μL of non-reducing SDS gel loading buffer and denaturation at 95 °C for 5 min. Finally, samples were separated by SDS-PAGE and analyzed by Western blot.

2.20. Single-cell transcriptome sequencing

ARP1 WT and ARP1 SAE1-OE cells in good condition were centrifuged at 1200 rpm for 5 min at 4 °C, washed twice with PBS, lysed with 1 mL of TRIeasy lysis solution, mixed by pipetting with a nuclease-free tip, transferred to a 1.5 mL nuclease-free EP tube, and then transcriptome sequencing was performed at Lianchuan Biotechnology Co.

2.21. Pristane oil-induced mouse plasmacytoma (MPC) model

Selecting male BALB/c mice aged 6−8 weeks (n = 18 mice in each group) and injecting AAV9 virus into the tail vein at a titer of 1×10^{10} VG/100 μL. After the virus injection, Pristane oil (2,6,10,12-tetramethylpentadecane) was injected intraperitoneally every 2 months with a dosage of 0.5 mL per injection for 3 injections. Cellular multinucleation and serum protein abnormalities were monitored in mice through Giemsa staining experiments and

serum electrophoresis. EV and AAV9-carried SAE1-OE vectors were purchased from GeneChem, Inc.

2.22. B cell transplant neoplasm (BTN) MM mouse model

We mated genetically engineered inbred strains of laboratory mice, the C57BL/6-lgs2em1(CAG-LSL-Myc) Smoc mice, and the B6.Cg-Commd10Tg (Vav1-icre) A2Kio/J mice, to activate the expression of Myc, a protooncogene, increasing the proclivity to malignant plasma cell transformation[24]. The spleens of the genetically modified mice offspring were removed, ground, and made into single-cell suspensions. Then, normal splenic B cells were purified using the MACS B220 mouse B cell sorting kit. After virus infection and CD4 Beads screening, these cells were divided into the control and SAE1-OE groups, which were injected into immunodeficient mice once more ($n = 10$ mice in each group).

2.23. 5TMM3VT mouse model

5TMM3VT mouse myeloma cells (1×10^6) were injected intravenously by tail vein into 8-week C57BL/KaLwrij mice. The mice were divided into 2 groups ($n = 10$ mice in each group). After 2 days, the control group was regurgitated with plain water and the experimental group with colchicine at 0.6 mg/kg twice weekly until the mice were sacrificed or died. Mice were sacrificed once they showed signs of hind limb weakness. The survival time of each group of mice was recorded.

2.24. MM xenograft model

We established MM xenograft models using 6−8-week SCID/NOD mice. 1×10^6 wild type (WT) and SAE1-OE cells were subcutaneously injected into the left and right ventral flank of the mice ($n = 6$ mice in each group), respectively. Mice were then gavaged twice weekly with water and colchicine (0.6 mg/kg). The tumor diameters were determined every other day using calipers. Once the xenograft tumor reached 15 mm in diameter, the mice were executed. The tumors were collected, weighed and then the tumor tissue was photographed.

2.25. MM patient-derived tumor xenograft (PDX) model

The PDX model was derived from biopsies collected from an extramedullary tumor under the scalp of an MM patient at the Department of Haematology, The First Affiliated Hospital of Nanjing Medical University (Nanjing, China). Tumor sections were transplanted subcutaneously into 4−6-week male SCID/NOD mice ($n = 6$) under pentobarbital anaesthesia according to the method reported by Zhou et al[25]. Once the tumors reached 500 mm^3 in size, they were harvested and the tumor tissue was then divided into 2.5 mm × 2.5 mm × 2.5 mm slices and subcutaneously implanted again. After this process was replicated for three times and the tumor reached 100−150 mm^3, the mice were randomly classified into control and treatment groups and injected with water or colchicine and BTZ every two days.

2.26. CRC patient-derived tumor xenograft (PDX) model

The PDX was generated using the surgically removed tumor tissue from a patient with CRC at the Department of Proctology, Nanjing Hospital of Chinese Medicine Affiliated to Nanjing University of Chinese Medicine (Nanjing, China). The tumor slices were transplanted subcutaneously into 6-week-old NOD/SCID mice ($n = 6$ mice in each group) under anesthesia with 1% sodium pentobarbital. The tumors were collected once their sizes reached 500 mm^3, and subsequently the tumor tissues were divided into 2.5 mm × 2.5 mm × 2.5 mm pieces and subcutaneously implanted into the NOD/SCID mice again. This process was then repeated three times, and once the tumor size had reached 100−150 mm^3, the mice were randomly divided into the control (Ctrl), COL administration, BTZ administration, and COL + BTZ combination groups.

All animal experiments were conducted according to the Government-published recommendations for the Care and Use of Laboratory Animals, and were approved by the Institutional Ethics Review Boards of Nanjing University of Chinese Medicine (Ethics Registration No. 201905A003).

2.27. Colchicine treatment study in MM patients

Colchicine treatment studies in MM patients were performed by Dr. HongMing Huang from Affiliated Hospital of Nantong University (Nantong, China). The study was in accordance with the Declaration of Helsinki 2013, and approved by the institutional review board of the Affiliated Hospital of Nantong University (2022-K043-01). Informed consent was obtained from all patients. The study has also been registered at ClinicalTrials.gov (Identifier: NCT05802992).

2.28. Statistical analysis

All data are presented as the mean ± standard deviation (SD). Two-tailed Student's *t*-test (2 groups) and one-way ANOVA for multiple comparisons were used for multiple comparisons to determine significance between experimental groups. The Kaplan−Meier method and Log-rank test were applied to determine the survival rate of MM patients. $^*P < 0.05$, $^{**}P < 0.01$, and $^{***}P < 0.001$ indicate statistically significant differences.

3. Results

3.1. Elevated SAE1 levels are associated with poor survival of MM patients and promote MM malignancy in vitro and in vivo

We first verified the satisfactory and comparable anti-tumor effect of both colchicine and colcemid in MM cells with IC_{50} values of approximate 0.3−0.4 μmol/L in ARP1 cells and 0.1−0.7 μmol/L in H929 cells (Supporting Information Fig. S1). To identify the potential therapeutic targets of colchicine/colcemid in MM, we used the HuProt™ human proteome microarray and Cy5-labeled colcemid as fluorescent probes to screen for the protein targets binding to colcemid (Fig. 1A). Among the 39 positive proteins that potentially interacted with colcemid, we examined the gene expression profiling (GEP) cohort of MM patients to determine the potential targets in MM cells. We found that only SAE1 showed a significant increase in plasma cells from staged patients with monoclonal gammopathy of undetermined significance (MGUS, $n = 22$) and MM ($n = 69$) compared to normal plasma cells (NP, $n = 15$) ($P < 0.01$) (Fig. 1B). Furthermore, the level of SAE1 was significantly correlated with poor prognosis in MM patients from the total therapy 2 (TT2) ($P < 0.01$) and proteasome inhibition for extending remission (APEX) trials ($P < 0.05$)

cohorts (Fig. 1C and D). Similarly, the results of the IHC analysis showed that SAE1 levels were higher in MM primary samples than in normal tissues and positively correlated with Ki67, a key marker of cell proliferation ($P = 0.0001, R = 0.9966$) (Fig. 1E). Based on these findings, we hypothesized that SAE1 might be a potential therapeutic target in MM and proceeded to investigate its function in MM cells. Initially, we established SAE1 overexpression (SAE1-OE) MM cell lines (ARP1 and H929) using a lentiviral system and verified by Western blotting. The results of the CCK-8 assay showed that the overexpression of SAE1 promoted the proliferation of MM cells (Fig. 1F). The results of the BrdU staining assay revealed that SAE1-OE cells were characterized by a lower fraction of G0/G1 stage in the cell cycle compared to WT cells, indicating that SAE1-OE cells were rapidly proliferating (Fig. 1G). In agreement with the above result, the colony formation assay revealed that SAE1-OE cells also showed increased long-term cell growth compared to WT cells (Fig. 1H). In contrast, knocking down SAE1 using lentiviral expression of shRNA (SAE1-KD) or siRNAs inhibited cell proliferation (Fig. 1I and Supporting Information Fig. S2) and cell cycle progression without inducing apoptosis (Fig. 1J). Moreover, the long-term proliferation ability of SAE1-KD cells was weaker than control cells (Fig. 1K). Additionally, the CCK-8 assay showed a relatively lower IC_{50} value of colchicine/colcemid in SAE1-OE cells (ARP1: 44.8-48.5 nm, H929: 71.4-95.4 nm) compared to control MM cells, indicating the potential of SAE1 to sensitize MM cells to colchicine/colcemid in cell proliferation (Fig. S1A−S1D).

To validate these findings *in vivo*, we utilized two mouse models: the chemically induced mouse plasmacytoma (MPC) model and the B cell transplant neoplasm (BTN) MM mouse model. The MPC model closely mimics human MM regarding tumor biology and phenotype. It was established by repeatedly injecting pristane into the BALB/c mice intraperitoneally (Fig. 1L; STAR Methods). Approximately 120 days after the first injection of pristane, we observed the development of ascites and the characteristic tumor plasma cells/field in the ascitic fluid (Supporting Information Fig. S3A). We also detected abnormalities in serum protein electrophoresis (Fig. S3B) and the expression of SAE1 in the spleen (Fig. S3C). The survival period of pristane-induced MPC mice was further shortened after overexpressing SAE1 using an AAV9 virus infection method (Fig. 1M). Their ascites cells expressing CD138, a hallmark of mature plasma and myeloma cells, indicated an oncogenic role of SAE1 in MM (Fig. 1N). Similarly, the survival period of BTN MM model mice, obtained by transplanting purified normal or modified splenic B cells from transgenic *Myc*$^{+/+}$*&Vav-icre* mice into immunodeficient mice once more (Fig. 1O; STAR Methods), was significantly reduced due to SAE1 overexpression (Fig. 1P). Additionally, IHC staining of the mouse tibia section showed a significant increase in typical MM indicators, such as CD138 and Ki67, in the SAE1-OE group (Fig. 1Q). MicroCT (μCT) imaging of the bone density and volume revealed severe bone damage in the SAE1-OE group, with a considerable reduction in bone mineral density (BMD) compared to the WT group at the end of the experiment (Fig. 1R and S3D). These results demonstrate that SAE1, a potential new therapeutic target identified in this study, promotes MM cellular malignancy.

3.2. SAE1 induces p27 nuclear export and promotes MM malignancy via SUMOylating p27

To elucidate the regulatory mechanism of SAE1 in MM, we conducted a Co-IP assay using SAE1 and SUMO1 antibodies and identified downstream targets of SAE1 or SUMOylation through MS. The unified GO (gene ontology) enrichment analysis supported the involvement of the cell cycle and regulation of the cell cycle in the SAE1-mediated proliferation of MM (Fig. 2A). Intriguingly, we observed an abnormal increase in the expression of p27, a classic tumor-suppressing gene and regulator of the G0/G1 cell cycle phase, in SAE1-OE cells and a decrease in SAE1-KD cells out of ordinary (Fig. 2B and C). This finding was further supported by a positive correlation between SAE1 and p27 expression in primary samples from MM patients (Fig. 2D). Notably, p27 was mislocalized in the cytoplasm of SAE1-OE cells, unlike its normal localization in the nucleus (Fig. 2E). This mislocalization may hinder its suppressive function in regulating cell proliferation, as p27 is known to act as a gatekeeper for the G1/S transition and G2/M progression in the most common and lethal human epithelial cancer[26]. Therefore, the cytoplasmic mislocalization of p27 may block its nuclear suppressive function during cellular proliferation in cancer cells[27-29]. Cytoplasmic mislocalization might partially explain the total increase in p27 levels due to the relatively lower ubiquitin-mediated degradation in SAE1-OE cells, as shown by the Co-IP assay and treatment with the proteasome inhibitor MG132 (Supporting Information Fig. S4A). Immunofluorescence (IF) staining results further confirmed that p27 was highly expressed in the cytoplasm of SAE1-OE cells compared to WT cells (Fig. 2F), as supported by the nucleocytoplasmic protein separation assay in SAE1-OE and SAE1-KD MM cells (Fig. 2G and H). These findings suggest that SAE1 may interact with p27, affecting its localization in cancer cells. This interaction was confirmed by the Co-IP assay using SAE1-Flag or p27 antibodies as bait (Fig. 2I). The GST pull-down assay showed a direct interaction between SAE1 and p27 (Fig. 2J), suggesting that p27 may be a client protein of SAE1 modification that promotes MM cell growth.

We predicted two potential lysine residues (K134 and K190) as potential SUMOylation sites for p27 using the website (http://sumosp.biocuckoo.org/online.php) and examined them through double mutation (DM) arginine version (K134R/K190R, p27-DM) (Fig. 2K). The mutation of these two sites decreased the expression level of p27 in MM cells under both single (p27-DM) and co-transfection (p27+SAE1) conditions, compared to the control and weakened the antagonistic effect of SAE1 on the degradation of ubiquitinated p27 (Fig. 2L and Fig. S4B). The results of the nucleocytoplasmic separation assay further supported that p27-DM attenuated the regulatory effects of SAE1 on p27 nuclear export (Fig. 2M). This finding was also confirmed by IF staining assays (Fig. 2N). Interestingly, we observed that the mutation of the p27 SUMOylation sites (p27-DM-GFP) almost completely prevented the translocation of p27 out of the cell nucleus, even in SAE1-OE cells (Fig. 2O and Supporting Information Movies). To confirm the direct modification of p27 by SAE1, we performed *in vitro* SUMOylation assays and found that p27-DM weakened the SUMOylation level of the purified p27 protein (Fig. 2P). Furthermore, the cell co-transfection-based SUMOylation assay showed that SAE1 enhanced p27 SUMOylation *in vivo*, which was abrogated by the K134R/K190R mutation (Fig. 2Q) or knockdown method (Supporting Information Fig. S5A and S5B). We ordered four siRNAs targeting p27 and tested their effectiveness. We also transiently transferred p27-DM plasmids to rescue the expression of p27 in corresponding cells (Fig. S5C). Subsequently, we selected the siRNA with the best effect for further experiments (Fig. S5D). The proliferation of MM cells was tested using the CCK-8 assay

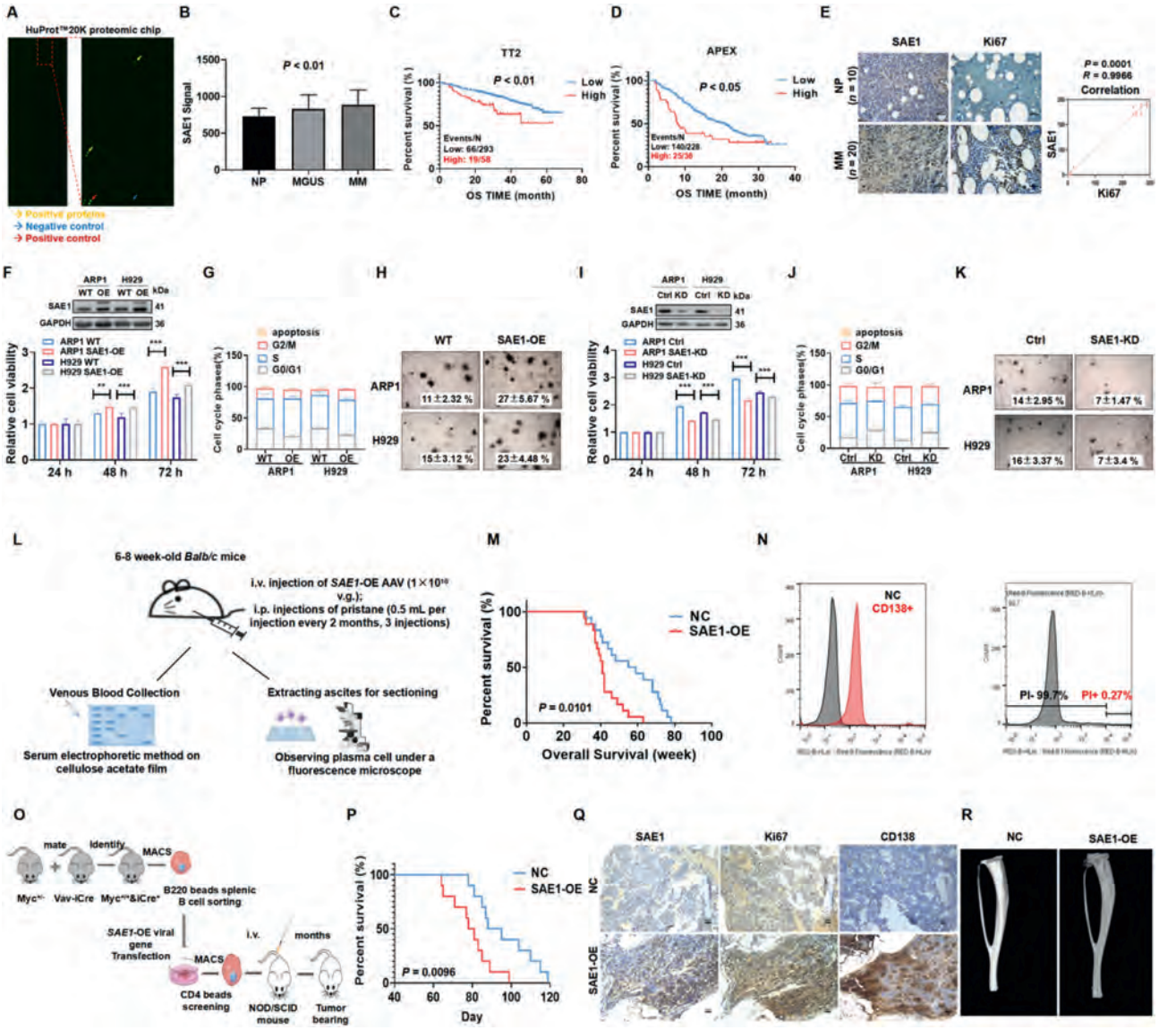

Figure 1 Elevated SAE1 levels are associated with poor survival of MM patients and promote MM malignancy *in vitro and in vivo.* (A) The HuProt™ 20 K proteomic chip shows protein-target binding to colcemid. Yellow arrows indicate positive protein interaction with colcemid, red arrows indicate positive control, and blue arrows indicate negative control (BSA). (B) The levels of *SAE1* mRNA were significantly increased in MM patient samples. The *Y*-axis shows the signal level of SAE1, while the *X*-axis represents the groups of healthy donors with normal BM plasma cells (NP; $n = 15$), monoclonal gammopathy of undetermined significance (MGUS; $n = 22$), and multiple myeloma (MM; $n = 69$) are shown on the *X*-axis, respectively. (C, D) An increase in the expression of *SAE1* mRNA was closely linked to poor overall survival (OS) at first diagnosis and after treatment of MM patients from the (C) TT2 and (D) APEX patient cohorts, respectively. (E) Representative immunohistochemistry (IHC) staining of primary MM ($n = 20$) and NP samples ($n = 10$); scale bar: 100 μm. (F) Western blotting (WB) assays detected the expression of SAE1 in WT and SAE1-OE MM cells, and CCK-8 assay evaluated the proliferation ability of WT and SAE1-OE MM cells. (G) BrdU staining assay showed that the proportion of G0/G1 phase decreased significantly in SAE1-OE cells compared to that in WT cells. (H) Representative images of cell colonies of WT and SAE1-OE cells in soft agar. (I) WB assays assessed the expression of SAE1 upon transfection with SAE1-targeting shRNAs, and CCK-8 assay evaluated the proliferation rate of SAE1-KD and Ctrl MM cells. (J) The BrdU staining assay determined the cell cycle of Ctrl and SAE1-KD MM cells. (K) Representative images of cell colonies of Ctrl and SAE1-KD cells in soft agar. (L) A diagrammatic representation of the pristane oil (2,6,10,12-tetramethylpentadecane)-induced mouse plasmacytoma (MPC) model. (M) The overexpression of SAE1 significantly shortened the survival time of the MPC mouse model ($n = 18$ in each group). (N) The ascites cells expressed CD138. (O) Schematic representation of tumor induction and analysis. The experimental method relied on the adoptive transfer of B220+ B cells obtained from the spleens of 5−8-week-old CD45.2+ double transgenic $Myc^{+/+}$&$icre^{+}$mice. Donor B cells were isolated using the MACS B220 mouse B cell kit (Miltenyi Biotec), transfected with a high-titer SAE1 virus solution for 48 h *in vitro*, and transferred to NOD/SCID mice, using various immunological, imaging, and histopathological methods to analyze tumors arising in B-cell recombinant hosts. (P) The overexpression of SAE1 significantly shortened the survival time of the BTN MM model mice ($n = 10$ in each group). (Q) Representative IHC staining of histological sections of bones in the NC and SAE1-OE groups; scale bar: 100 μm. (R) Representative microCT images of bones in the NC and SAE1-OE groups. The data are expressed as the mean ± SD; $^{*}P < 0.05$, $^{**}P < 0.01$, and $^{***}P < 0.001$.

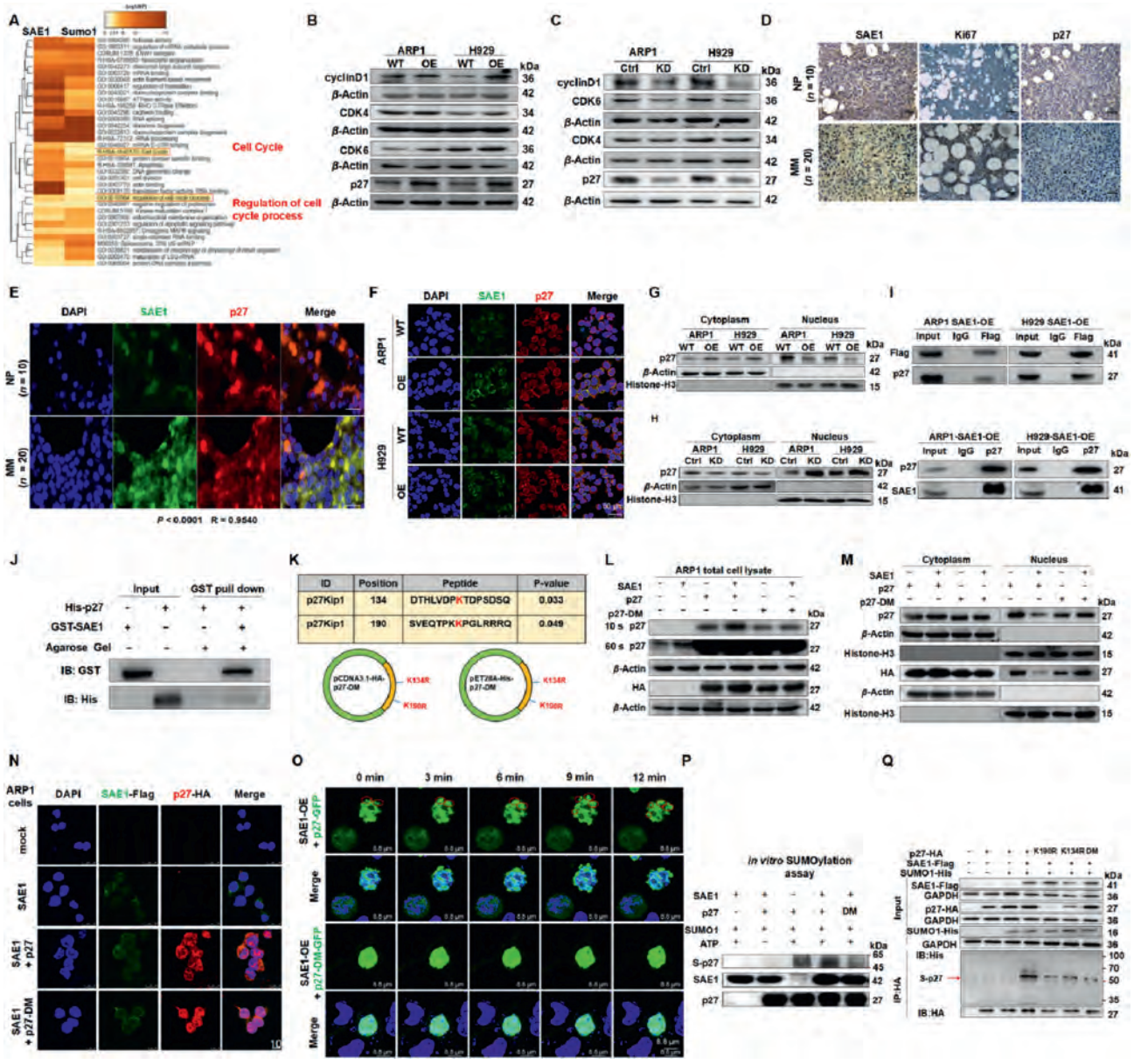

Figure 2 SAE1 induces p27 nuclear export and promotes MM malignancy *via* SUMOylating p27. (A) The GO molecular functions closely related to the proliferation of ARP1 WT and SAE1-OE cells were identified by Co-IP-MS analysis. (B, C) The results of the WB analysis showed the expression of G0/G1 phase-related cyclins in SAE1-OE (B) and SAE1-KD cells (C). (D) Representative IHC staining of primary MM ($n = 20$) and NP samples ($n = 10$); scale bar: 100 μm. (E) Immunofluorescence (IF) assay of SAE1 and p27 expression in samples of NP and MM patients; scale bar: 50 μm. (F) The p27 protein was highly expressed in the cytoplasm of SAE1-OE ARP1 and H929 cells, as determined by IF staining for SAE1 and p27; scale bar: 50 μm. (G, H) The cytoplasmic expression of p27 increased, while nuclear expression decreased in SAE1-OE MM cells. In contrast, the cytoplasmic expression of p27 decreased significantly, while nuclear expression increased in SAE1-KD MM cells. (I) Co-IP experiments showed that SAE1 interacted with p27 in ARP1 and H929 cells. (J) GST pull-down assays showed that SAE1 was directly associated with p27 in ARP1 and H929 cells. (K) The p27-K134 & K190 amino acid residues were predicted to be the major SUMOylation sites of p27. A p27 double-mutant plasmid was constructed using the recombinant plasmid method. (L) The results of WB analysis showed that two major SUMOylation sites, including p27-K134 & K190, were mutated, resulting in decreased p27 expression in ARP1 cells. (M) Nucleocytoplasmic separation analysis showed that mutations in the two major SUMOylation sites of p27-K134 & K190 decreased the nuclear export of p27 in ARP1 cells. (N) The mutation of p27-K134 & K190 sites significantly reduced SAE1-mediated nuclear export in ARP1 cells; scale bar: 10 μm and 25 μm. (O) Time-lapse imaging results of cells co-overexpressing SAE1 and p27/p27-DM under a confocal microscope and representative pictures indicated that the mutation of the p27 SUMOylation sites almost abolished the translocation of p27 out of the cell nucleus (see Supporting Information Movies); scale bar: 8.8 μm. (P) *In vitro* SUMOylation of wild-type and lysine-to-arginine double-mutant forms of p27 showed that double mutants weakened the SUMOylation of p27 by SAE1. (Q) *In vivo* SUMOylation of wild-type and lysine−arginine double mutant forms of p27 indicated that double mutants attenuated the SUMOylation of p27 by SAE1 in ARP1 WT cells.

in the following groups: WT, SAE1-OE, SAE1-OE/p27-KD, and SAE1-OE/p27-KD/p27-DM (Fig. S5E). Our study suggests that the two lysines in p27 (K134 and K190) are most likely to be SUMOylated. Therefore, we used mutant p27 plasmids in which the two lysines were substituted with arginines (p27-DM) to replace the endogenous p27 in MM cells. After removing the key SUMOylation sites in p27, the proliferation ability of SAE1-OE cells significantly decreased. These results demonstrate that SAE1 can directly bind and SUMOylate p27 to facilitate its nuclear export.

3.3. SAE1 promotes p27 LLPS through SUMOylation of p27 leading to p27 nuclear export eventually

While exploring the mechanism by which SAE1 causes p27 nuclear export, we found that the p27 protein contains intrinsically disordered regions (IDRs) often modified post-translationally (such as through phosphorylation) and exhibit LLPS properties[30]. Therefore, we investigated the relationship between LLPS and SUMOylation of p27 mediated by SAE1. To identify self-assembling and partner-dependent phase-separating proteins, including p27, we utilized PhaSePred (http://predict.phasep.pro/detail/P46527/), a meta-predictor for integrating LLPS scores from various PS-related prediction tools (PS-Self score = 0.796, Rank = 0.934) (Fig. 3A). To further investigate the effect of SUMOylation on the LLPS phase of p27, we simultaneously expressed p27-GFP and p27-DM-GFP fusion proteins in live MM cells. We observed that p27-GFP cells formed more distinct speckle-like droplets than p27-DM-GFP cells (Fig. 3B), indicating that SUMOylation modifications may affect the LLPS phase of p27. To confirm the SUMOylation of p27 inducing LLPS formation, we performed an *in vitro* droplet assay and demonstrated that the addition of *in vitro* purified recombinant p27-GFP and p27-DM-GFP fusion proteins to buffers containing 10% PEG-8000 resulted in the solution opaque solutions with droplet aggregation, whereas equivalent solutions with only GFP remained transparent (Fig. 3C; STAR Methods). In addition, we found that the p27-GFP formed droplets at a minimum concentration of 0.5 μmol/L, and the droplets increased in a dose-dependent manner in the presence of PEG8000 *in vitro*, which could be eliminated by increasing the concentration of NaCl (Fig. 3D and E). We then added purified SAE1 to the p27-GFP or p27-DM-GFP systems and observed that activating SUMOylation significantly promoted LLPS formation of p27-GFP at a low concentration, while the formation of p27-DM-GFP was less affected (Fig. 3F). Summarily, SAE1 delayed the NaCl-induced abrogation of LLPS of p27-GFP (Fig. 3G) by mediating p27 SUMOylation.

To assess the relationship between LLPS and the nuclear export of p27, we used the nuclear export inhibitor KPT-330 in live MM cells. We observed that the formed p27 spots were located near the nucleus, as indicated by staining with Hoechst 33342 (Fig. 3H). Additionally, the results of the fluorescence recovery after photobleaching (FRAP) assay indicated a significant difference in the fluorescent recovery rate between p27-GFP and p27-DM-GFP in HEK293 cells. Specifically, the recovery rate of p27-GFP was much faster than that of p27-DM-GFP (Fig. 3I; STAR Methods). We also examined how p27 was exported by detecting chromosome region maintenance 1 (CRM1), also known as exportin 1 (XPO1), which acts as a nuclear export receptor and directly conjugates nuclear export signals from cargo proteins to transport them to the cytoplasm[31]. The results of the Co-IP assay showed an interaction between p27 and CRM1 in two MM cells using p27 antibodies as bait (Fig. 3J). However, the double mutation of p27 (p27-DM) decreased its ability to bind to CRM1 (Fig. 3K). While the nuclear export inhibitor KPT-330 had a minimal effect on the total expression of p27, it did trap more p27 localized in the nucleus, particularly in SAE1-OE MM cells (Fig. 3L and M). Thus, KPT-330 decreased the proliferation rate of MM cells induced by SAE1/p27 overexpression (Fig. 3N). These findings were further supported by IF staining (Fig. 3O), which showed that SAE1 promoted LLPS of p27 by SUMOylation, and enhanced its binding to CRM1 near the nuclear membrane for nuclear export, thus promoting MM cellular malignancy.

3.4. Colchicine inhibits MM malignancy by directly targeting the E74 site of SAE1

Our research has demonstrated the oncogenic role of SAE1 in MM. We then obtained the first crystalized monomer of SAE1 through X-ray and deposited it in the PDB database (PDB: 8VY5). Using colcemid as a probe, we screened SAE1 and further investigated its binding with colcemid or colchicine to SAE1 through virtual molecular docking. The most probable binding site of SAE1, as predicted by Sitemap, is shown in Fig. 4Aa. In the case of colcemid (Fig. 4Ab), the amino group of colcemid forms a hydrogen bond with E74 of SAE1, while colchicine binds to SAE1 in a similar manner (Fig. 4Ac). Notably, the side chain of C133 interacts with the methoxy group of colcemid in the binding pocket. To specifically target cysteine residues in the SAE1 protein, we designed a covalent warhead that forms covalent bonds with the protein. LC/MS experiments were carried out to validate the binding site of the covalent ligand. C133 and three other cysteine residues (C14, C214, and C303) were identified as the target residues in IAA-peptides and Cpd-peptides (Fig. 4B; STAR Methods). Virtual molecular docking suggests that the covalent ligand interacts with E74 and T72 and forms a hydrogen bond with D256, while the covalent bond with C133 has also been identified (Fig. 4C). These results indicate the direct binding of colcemid/colchicine into the pocket of SAE1. Interestingly, the results of the MST assay showed that colchicine exhibited a higher affinity for SAE1 (K_d = 2.56 μmol/L) than colcemid (K_d = 70.49 μmol/L) (Fig. 4D). Furthermore, using isothermal titration calorimetry (ITC), we found that $SAE1^{E74A}$ showed a 314-fold decrease in the affinity for colchicine compared to wildtype SAE1 (Fig. 4E and F). In summary, E74 plays a critical role in binding SAE1 to colcemid/colchicine.

Since colchicine had a higher binding affinity to SAE1 than colcemid, we further investigated its anti-cancer effect on MM cells. Protein blot analysis was performed on MM cells, and the results showed that colchicine inhibited cell proliferation by decreasing the total expression of p27 and inhibiting nuclear export in cells without altering the total expression of the SAE1 protein (Fig. 4G and H). Additionally, colchicine inhibited the long-term proliferation of SAE1-OE cells, as determined by the colony formation assay (Fig. 4I). The G0/G1 phase ratio of arrested cells significantly increased after colchicine treatment (Fig. 4J), and SAE1-OE cells were more sensitive to colchicine-induced apoptosis (Fig. 4K). To determine the effect of colchicine on the modification of p27 by SAE1, we performed *in vitro* SUMOylation assays with and without colchicine treatment. The results showed that colchicine disrupted the SUMOylation of p27 by targeting SAE1, and the E74A mutation of SAE1 also attenuated the regulation of SUMOylation of p27 (Fig. 4L). A Co-IP

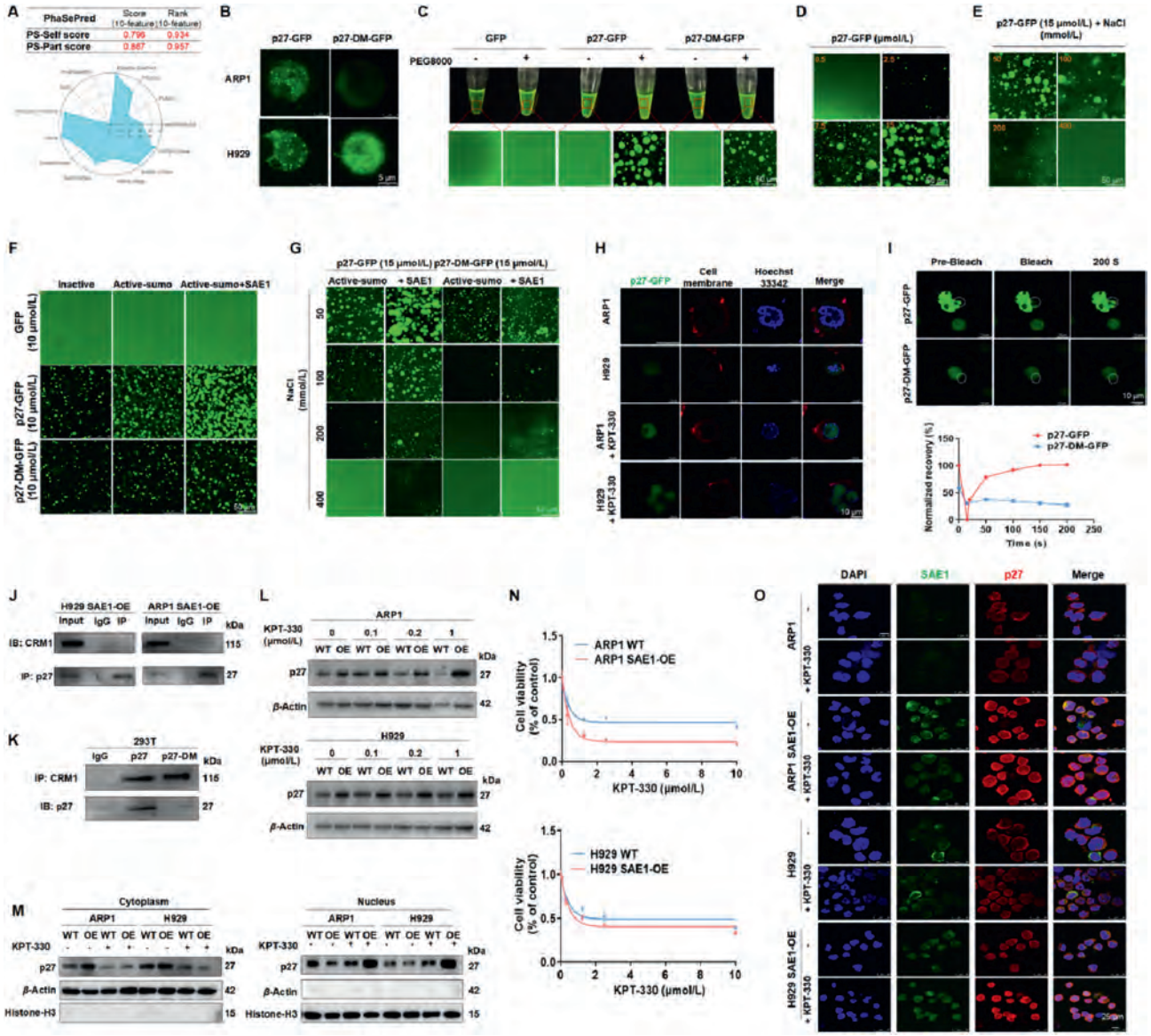

Figure 3 SAE1 promotes p27 LLPS through SUMOylation of p27 leading to p27 nuclear export eventually. (A) The intrinsically disordered region of the p27 protein was predicted using a meta-predictor for phase-separating proteins PhaSePred (see http://predict.phasep.pro/detail/P46527/). (B) The phase-separated formation of wild-type p27-GFP and double-mutant SUMOylation sites of p27-DM-GFP in ARP1 and H929 cells ($n = 3$ biologically independent experiments); scale bar: 5 μm. (C) The visualization of turbidity associated with droplet formation. Tubes containing GFP (left pair) or p27-GFP (middle) and p27-DM-GFP (right pair) in the presence (+) or absence (−) of PEG-8000 ($n = 3$ biologically independent experiments); scale bar: 50 μm. (D) Representative images of droplet formation of p27-GFP at various protein concentrations ($n = 3$ biologically independent experiments); scale bar: 50 μm. (E) Representative images of p27-GFP droplet formation at 15 μmol/L protein concentration with different salt concentrations ($n = 3$ biologically independent experiments); scale bar: 50 μm. (F) Representative images of droplet formation of GFP-vector or p27-GFP and p27-DM-GFP with (+) or without (−) SAE1 added *in vitro* with activated or non-activated SUMOylation, respectively ($n = 3$ biologically independent experiments). (G) Representative images of droplet formation of p27-GFP or p27-DM-GFP in the presence (+) or absence (−) of different salt concentrations of SAE1 under conditions that activate SUMOylation *in vitro* ($n = 3$ biologically independent experiments); p27-GFP or p27-DM-GFP was added to the droplet formation buffer to achieve 15 μmol/L protein concentration with a final NaCl concentration as indicated; scale bar: 50 μm. (H) Spots formed by the p27-GFP fusion protein aggregated in the cytoplasm of ARP1 and H929 cells, and the nuclear export inhibitor KPT-330 restricted the aggregation of spots to the cytoplasm; scale bar: 10 μm. (I) Kinetic recovery times of bleached GFP-tagged p27 droplet foci in HEK293 cells compared to p27-DM, as determined by laser at 488 nm; scale bar: 10 μm. (J) The Co-IP experiments confirmed the interaction of p27 and CRM1 in ARP1 and H929 cells using p27 antibodies as bait. (K) The results of a Co-IP analysis showed that the interaction between p27 and CRM1 was weakened due to the double-site mutation of p27-DM (K134R/K190R). (L) KPT-330 did not affect the total protein expression of p27 in ARP1, H929 WT, and SAE1-OE cells. (M) KPT-330 inhibited the nuclear export of p27 in ARP1, H929 WT, and SAE1-OE cells, as shown by nucleocytoplasmic separation analysis. (N) KPT-330 decreased the proliferation of MM cells caused by SAE1/p27 *in vitro*. (O) KPT-330 repressed the nuclear export of p27 in ARP1 and H929 WT and SAE1-OE cells by IF staining for SAE1 and p27 ($n = 3$ biologically independent experiments); scale bar: 25 μm. The data are expressed as the mean ± SD.

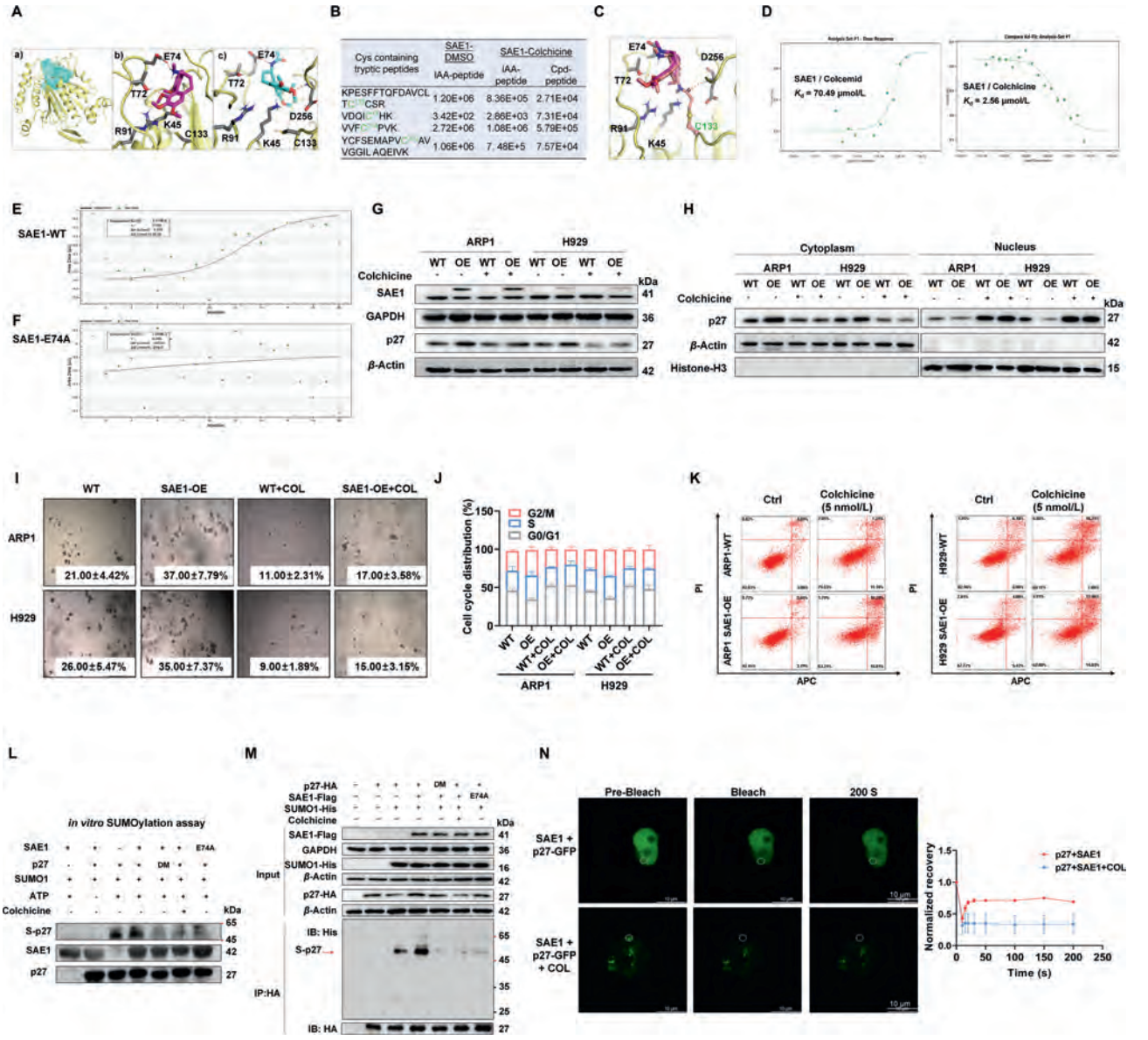

Figure 4 Colchicine inhibits MM malignancy by directly targeting the E74 site of SAE1. (A)The potential binding site (a, in blue mesh) of SAE1 with colcemid (b, in magenta sticks) or colchicine (c, in blue sticks) in SAE1 crystal structure. SAE1 is represented as a pale-yellow cartoon, and hydrogen bonds are shown as red dotted lines. Key residues are shown as grey sticks. (B) The results of covalent mass spectrometry sequencing. (C) Predicted binding mode of covalent ligand binding with SAE1. (D) MST analysis for the interaction between colcemid/colchicine and human SAE1 recombination protein. (E, F) ITC results of colchicine on wild-type SAE1 (E) and site-directed mutagenesis (F) indicated that SAE1−74 interacted with colchicine *via* hydrogen bonds. (G) The results of WB analysis indicated that colchicine inhibited the expression of p27 but not the expression of SAE1 in MM cells. (H) Nucleocytoplasmic segregation analysis suggested that colchicine inhibited p27 nuclear export caused by SAE1 in MM cells. (I) Representative images of colchicine on cell colonies of ARP1 and H929 cells with or without the overexpression of SAE1 in soft agar. (J) Flow cytometry assays confirmed that the proportion of cells in the G0/G1 phase significantly increased in the dosed group compared to those in the non-dosed group. (K) Colchicine (5 nmol/L) treatment in ARP1 and H929 cells for 48 h was performed to evaluate its effect on apoptosis. (L) *In vitro* SUMOylation of colchicine co-incubation treatments and the glutamic-to-alanine mutant form of the SAE1−74 site indicated that colchicine and mutation attenuated p27 SUMOylation by SAE1. (M) *In vivo* SUMOylation of the colchicine co-incubation treatment and SAE1−74 site glutamate-to-alanine mutant form suggested that colchicine and the mutant weakened the SUMOylation of p27 by SAE1. (N) The Fluorescence recovery after photobleaching (FRAP) showed the kinetic recovery times of bleached GFP-tagged p27 droplet foci in HEK293 cells with or without colchicine treatment ($n = 3$ biologically independent experiments), as determined by laser at 488 nm; scale bar: 10 μm. The data are expressed as the mean ± SD.

assay showed that colchicine treatment on MM cells attenuated the SUMOylation of p27 induced by SAE1, and SAE1-E74 was identified as a critical site-specific target of colchicine to interfere with the SUMOylation of p27 (Fig. 4M). Furthermore, the FRAP assay and IF staining showed that the colchicine treatment could repress the LLPS of p27-GFP (fluorescent recovery rate) and the cytoplasmic localization in HEK293 cells, respectively (Fig. 4N and Supporting Information Fig. S6).

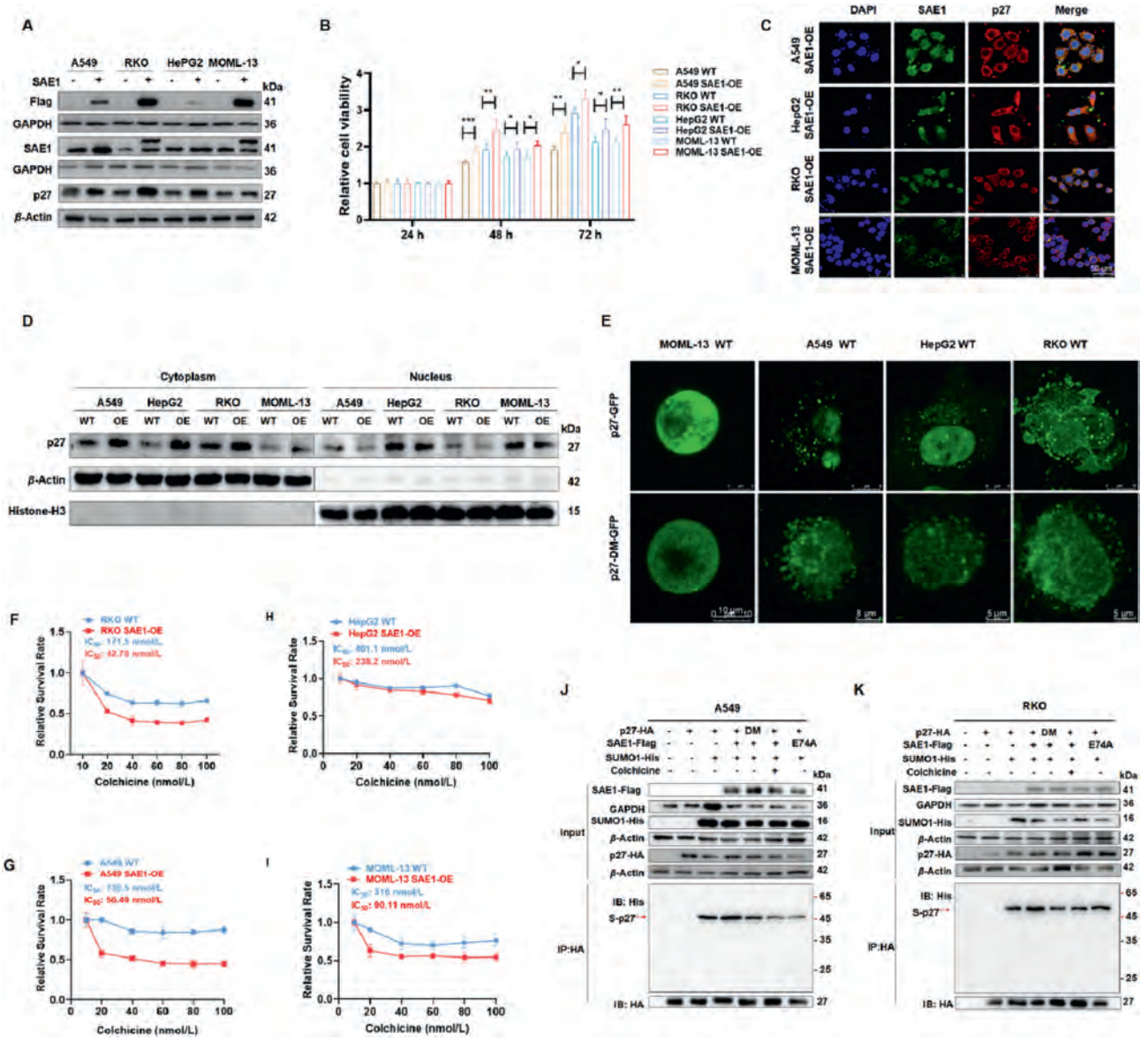

Figure 5 SAE1 promotes cellular malignancy in various types of cancer. (A) WB profiling revealed a correlation between the overexpression of SAE1 and p27 in various types of cancer. (B) CCK-8 assay determined the proliferative capacity of WT and SAE1-OE cells in different cancer types. (C) The co-localization of p27 with SAE1 in different types of cancer and high levels of p27 in the cytoplasm was determined by IF analysis; scale bar: 50 μm. (D) Nucleocytoplasmic isolation analysis showed that SAE1 overexpression in various cancer models resulted in the nuclear export of p27. (E) Phase-separated formation of wild-type p27-GFP and p27-DM-GFP in different types of cancer cells ($n = 3$ biologically independent experiments); scale bar: 5 μm, 8 μm, and 10 μm. (F−I) The effect of colchicine on the viability of A549, RKO, HePG2, and MOML-13 cells with/without SAE1 overexpression. (J, K) The results of an *in vivo* SUMOylation analysis indicated that SAE1 enhanced p27 SUMOylation, but not p27 in lysine−arginine double mutant form; either colchicine treatment or SAE1 in glutamate-alanine mutant form (E74A) weakened p27 SUMOylation in A549 (G) and RKO (H) cells. The data are expressed as the mean ± SD; $^{*}P < 0.05$, $^{**}P < 0.01$, and $^{***}P < 0.001$.

3.5. SAE1 promotes cellular malignancy in various types of cancer

To further extend the role of SAE1 as a pro-oncogenic driver in the growth of tumor cells through SUMOylation of p27, we conducted experiments to examine the effects of overexpressing SAE1 in lung cancer, colon cancer, liver cancer, and leukemia cells (Fig. 5A). We found that p27 levels were increased in these four SAE1-OE cancer cells with enhanced cellular proliferation (Fig. 5B). IF experiments revealed that SAE1 co-localized with p27, while p27 was mainly expressed in the cytoplasm of the four SAE1-regulated cancer cells (Fig. 5C). Consistent with our previous findings in MM cells, we also observed the mislocalization of p27 in the cytoplasm using a nucleocytoplasmic separation assay (Fig. 5D). Furthermore, our results suggest that SAE1 may regulate p27 in various types of cancer through two previously identified SUMOylation sites, as evidenced by the antagonistic effect of SAE1 on ubiquitin-mediated degradation of p27-DM (Supporting Information Fig. S7A and S7B). Additionally, we observed that p27-GFP formed more discrete spots than p27-DM-

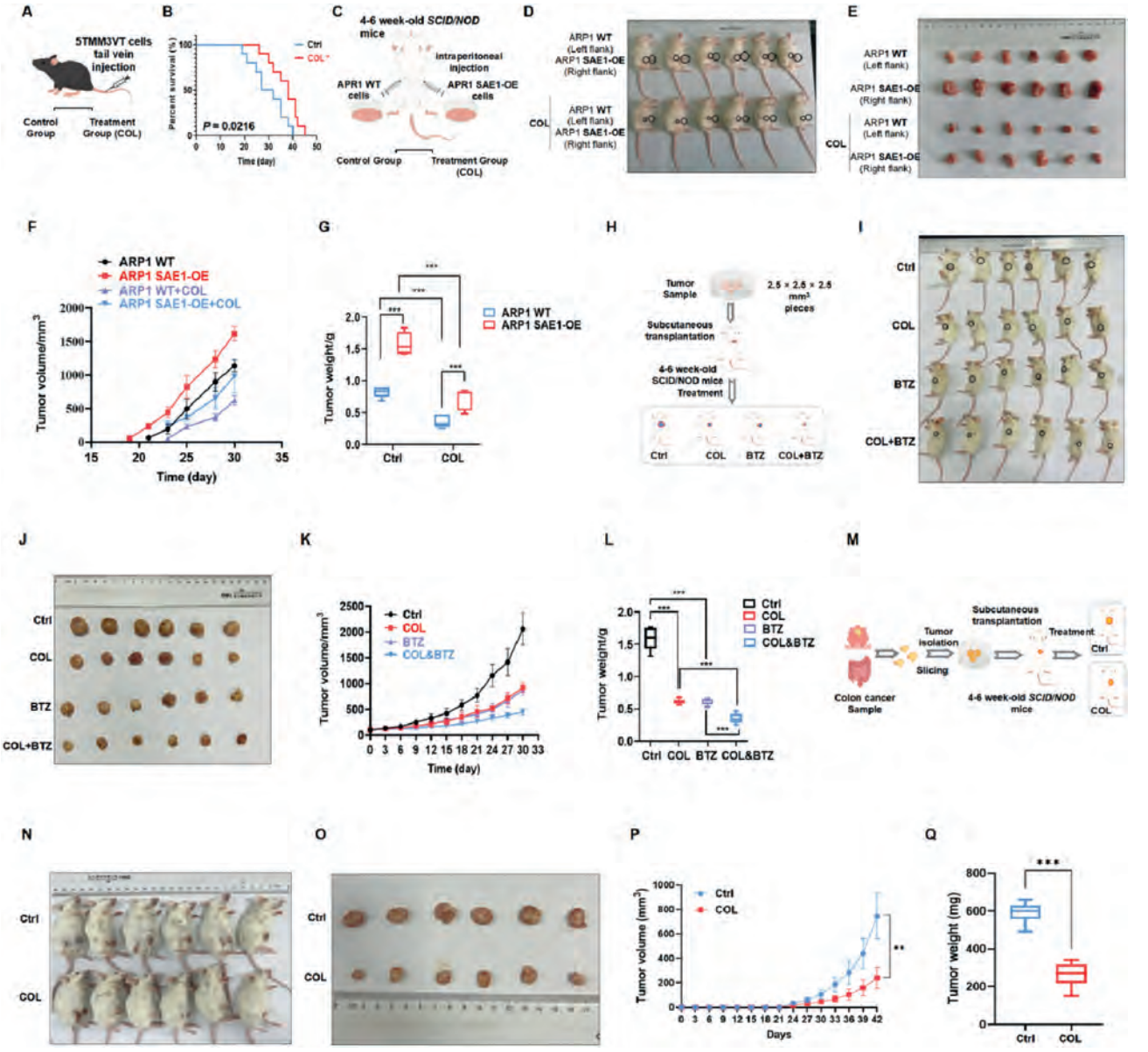

Figure 6 Colchicine inhibits tumor progression in multiple models *in vivo*. (A) The diagrammatic representation of the 5TMM3VT MM mouse model. (B) Treatment with colchicine significantly prolonged the survival of 5TMM3VT mice ($n = 10$ in each group). (C) A subcutaneous xenograft tumor mouse model. (D, E) Images of xenografts from different groups of NOD/SCID mice ($n = 6$ in each group). (F) The time course of tumor growth in NOD/SCID mice injected with ARP1 WT/SAE1-OE cells, with or without colchicine treatment. (G) The average tumor weight of ARP1 WT/SAE1-OE xenografts in the colchicine-treated and untreated groups on Day 32 after MM cell inoculation. (H) A map of the MM PDX model. (I, J) Photographs of tumors with and without colchicine and BTZ treatment from several groups of MM PDX model mice ($n = 6$). (K) The tumor growth curves of different groups of MM PDX models. (L) The average tumor weight in different groups of the MM PDX model. (M) The diagrammatic representation of the colon cancer PDX model. (N, O) Images of patient-derived xenografts from different groups of NOD/SCID mice ($n = 6$). (P) The time course of tumor growth in NOD/SCID mice injected with human colorectal carcinoma tissue, with or without colchicine treatment. (Q) The average tumor weight of patient-derived xenografts with or without colchicine treatment on Day 42 after injection. The data are expressed as the mean ± SD; $^{*}P < 0.05$, $^{**}P < 0.01$, and $^{***}P < 0.001$.

GFP in all four types of cancer cells (Fig. 5E), supporting the general mechanism of SUMOylation in promoting the entry of p27 into LLPS. Furthermore, the CCK-8 assays showed that colchicine effectively inhibited the proliferation of pan-cancer cells (170−400 nmol/L) and sensitized SAE1-OE cells (40−238 nmol/L) (Fig. 5F−I). Co-IP assay results showed that SAE1 increased the SUMOylation of p27 in lung and colon cancer cells using the p27-HA antibody, while treatment with colchicine or mutation of the SAE1-E74A site attenuated this effect (Fig. 5J and K). Our findings suggest that SAE1-mediated SUMOylation of p27 promotes its LLPS and nuclear export, leading to increased cellular proliferation, and that this process can be inhibited by colchicine through its binding to SAE1 in various types of blood and solid tumor cells.

Table 1 Baseline characteristics of the intention-to-treat population[a].

Characteristic	Colchicine group (n = 38)	Control group (n = 18)	Total (n = 56)
Age			
Median — year	59	60	59
Range — year	40–79	47–73	40–79
Distribution — no. of patients (%)			
18–64 year	24 (63.2)	11 (61.1)	35 (62.5)
≥65 year	14 (36.8)	7 (38.9)	21 (37.5)
ECOG performance status — no. of patients (%)[b]			
0 or 1	35 (92.1)	15 (83.3)	50 (89.3)
2	3 (7.9)	3 (16.7)	6 (10.7)
Cytogenetic risk at study entry — no. of patients (%)[c]			
High risk	14 (36.8)	7 (38.9)	21 (37.5)
Standard risk	24 (63.2)	11 (61.1)	35 (62.5)
Creatinine clearance			
Mean — mL/min	77.9 ± 17.8	80.7 ± 25.7	78.8 ± 20.2
Distribution — no. of patients (%)			
<60 mL/min	10 (26.3)	4 (22.2)	14 (25.0)
≥60 mL/min	28 (73.7)	14 (77.8)	42 (75.0)
Unknown or other value	0(0)		
Serum β2-microglobulin — no. of patients (%)			
<3.5 mg/L	23 (60.5)	10 (55.6)	33 (58.9)
≥3.5 mg/L	15 (39.5)	8 (44.4)	23 (41.1)
Previous regimens			
Median — no.	1	1	1
Range — no.	1–2	1–2	1–2
Distribution — no. of patients (%)			
1 regimen	28 (73.7)	14 (77.8)	42 (75.0)
2 or 3 regimens	10 (26.3)	4 (22.2)	14 (25.0)
Previous therapies — no. of patients (%)			
Bortezomib	28 (73.7)	12 (66.7)	40 (71.4)
Lenalidomide	6 (15.8)	4 (22.2)	10 (17.9)
Characteristic	Colchicine group (n = 38)	Control group (n = 18)	Total (n = 56)

[a]Plus–minus values are presented as mean ± SD.

[b]Eastern Cooperative Oncology Group (ECOG) performance-status scores range from 0 to 5, with 0 indicating no symptoms and higher scores indicating greater disability.

[c]The high-risk group consisted of patients with the genetic subtype t(4; 14) or t(14; 16) or with deletion 17p in 60% or more of plasma cells, according to central review of bone marrow samples obtained at study entry. The standard-risk group consisted of patients without t(4; 14) or t(14; 16) and with deletion 17p in less than 60% of plasma cells. The cut-off value of 60% for the proportion of plasma cells with deletion 17p was used on the basis of recommendations from the International Myeloma Workshop Consensus.

3.6. Colchicine inhibits cancer progression in multiple models in vivo

To assess the pharmacological effects of colchicine *in vivo*, we utilized the 5TMM3VT mouse model by injecting mouse 5TMM3VT cells into the tail vein of C57BL/KaLwRij mice. The administration of colchicine twice a week at a dose of 0.6 mg/kg each time significantly extended the survival of 5TMM3VT mice (P = 0.0216) (Fig. 6A and B; STAR Methods). The effect of colchicine *in vivo* was also tested in human MM cell line-derived xenograft (CDX) model (Fig. 6C; STAR Methods). Colchicine inhibited the growth of the MM CDX tumors and SAE1-OE MM cells showed increased sensitivity to colchicine treatment (Fig. 6D–G). Furthermore, we evaluated the effects of colchicine *in vivo* using the PDX model by transplanting patient-derived primary human MM xenografts into SCID/NOD mice (Fig. 6H; STAR Methods). Colchicine (0.6 mg/kg) was administrated by gavage twice a week, while the positive control drug bortezomib (BTZ, 1 mg/kg) was given twice a week *via* intraperitoneal injection. The results showed comparable anti-MM effects in suppressing the tumor volume and weight compared to the control group (Fig. 6I and J). Combination treatment with colchicine and BTZ was significantly more effective than single-treatment (Fig. 6K and L). The therapeutic effects of colchicine *in vivo* were also assessed in a colon cancer-related PDX model (Fig. 6M; STAR Methods). The SCID/NOD mice were transplanted with human colorectal carcinoma tissue and administered colchicine (0.6 mg/kg) by gavage twice a week, respectively. Consistently, colchicine showed an inhibitory effect on tumor growth (Fig. 6N–Q).

3.7. The application of colchicine enhances treatment responses and is positively correlated with progression-free survival of MM patients

At the clinical level, we conducted and evaluated the anti-cancer effects of colchicine on the progression of MM. Our cohort consisted of 56 patients, with 38 cases assigned to the Colchicine group and 18 cases assigned to the Control group. Almost all patients had previously been treated with BTZ or Lenalidomide. The patients in the two groups had similar baseline characteristics (see Table 1 and STAR Methods). Fig. 7A shows the hazard

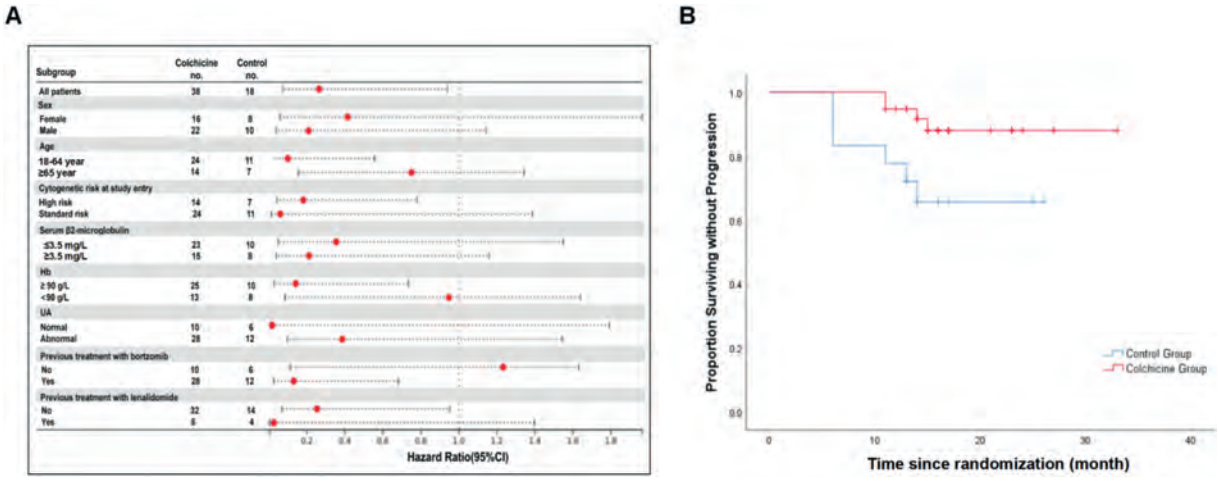

Figure 7 The application of colchicine enhances treatment responses and is positively correlated with progression-free survival of MM patients. (A) The hazard ratios and 95% confidence intervals for progression-free survival were calculated for prespecified subgroups based on the baseline characteristics. (B) The administration of colchicine significantly increased the survival time of patients compared to those in the control group.

ratios and 95% confidence intervals (CI) for progression-free survival in pre-specified subgroups based on the baseline characteristics. The treatment responses in the intention-to-treat population showed that MM patients benefited from the administration of colchicine, with an overall response rate of 78.8 (95% CI: 77.8−79.1) in the Colchicine group, which was higher than the response rate of 55.6 in the Control group. The difference in the clinical benefit rate between the two groups was significant (89.4, 95% CI: 89.1−90.0 in Colchicine group *vs* 61.1, 95% CI: 60.3−61.6 in Control group, $P = 0.013$) (see Table 2). Follow-up analysis showed a positive correlation between the application of colchicine and progression-free survival in MM patients (Fig. 7B) with manageable adverse events during the administration of colchicine in the safety-evaluable population (Supporting Information Table S2). These findings have important implications for future clinical trials and developing novel therapeutic methods targeting SAE1.

4. Discussion

Significant progress has been made in understanding and treating MM, including the use of CART therapy, however, it remains an incurable hematologic malignancy[32,33]. A more comprehensive understanding of the disease could potentially lead to the discovery of therapeutic targets that could benefit not only MM patients, but also those with other types of cancer. In this study, we used an alternative strategy to screen potential therapeutic targets by using toxic but bioactive natural compounds in Chinese medicine for anticancer therapy. By combining proteome microarray and microarray cohort data in MM to screen for and develop the potential therapeutic target(s) for toxic anti-tumor drugs, we identified and characterized the colchicine target, SAE1, which plays a crucial role in the SUMOylation PTM pathway. Our findings suggest that SAE1 may promote tumorigenesis in various types of cancer, including MM, colon cancer, etc. Intriguingly, we

Table 2 Treatment responses in the intention-to-treat population[a].

Variable	Colchicine group ($n = 38$)	Control group ($n = 18$)	P value
Best response — no. (%)[b]			
Complete response or better	6 (16.7)	2 (11.1)	0.640
Very good partial response or better	16 (42.1)	6 (33.3)	0.798
Partial response or better	30 (78.9)	9 (55.6)	0.028
Minimal response or better	34 (89.5)	11 (61.1)	0.013
Stable or progressive disease	4 (10.5)	7 (38.9)	0.013
Overall response rate — % (95% CI)[c]	78.8 (77.8−79.1)	55.6 (54.9−56.1)	
Clinical benefit rate — % (95% CI)[d]	89.4 (89.1−90.0)	61.1 (60.3−61.6)	0.013
Time to response — month			
Mean	1.6 ± 0.1	2.3 ± 0.2	
Median	1.5	2.3	

[a]Treatment responses were assessed by an independent review committee. Plus−minus values are presented as mean ± SD. CI denotes confidence interval.

[b]A stringent complete response was defined by a negative immunofixation test for myeloma protein in serum or urine and the disappearance of any soft-tissue plasmacytomas, with less than 5% plasma cells in the bone marrow, a normal serum free light-chain ratio, and an absence of clonal cells in the bone marrow.

[c]Overall response was defined as a partial response or better.

[d]Clinical benefit was defined as a minimal response or better.

disclosed a novel mechanism of how tumor cells escaped from the growth-inhibiting effects of the tumor suppressor p27. Contrary to the commonly accepted belief that tumor suppressor genes are down-regulated at the gene and protein levels, our research has shown that SAE1 increases the SUMOylation of p27, leading to an up-regulation of p27 expression in cancer cells. It is important to note that this SUMOylation does not affect the stability of the p27 protein, but rather its distribution within the cell. Our findings suggest that the SUMOylation of p27 by SAE1 allows for forming distinct patches of p27 near the nuclear membrane, ultimately promoting their export from the nucleus in various types of cancer.

Our work suggests that targeting the SUMO pathway and inhibiting the nuclear export of tumor suppressor proteins may be a promising treatment strategy for cancer. For example, UBE2I, a member of the E2 ubiquitin-conjugating enzyme family, catalyzes the formation of poly-SUMO chains and is essential for nuclear architecture and chromosome segregation. TAK-981, a synthesized inhibitor targeting UBE2I, is currently being tested in patients with metastatic solid tumors and lymphomas and has shown promising results as an anticancer treatment (ClinicalTrials.gov Identifier: NCT03648372)[34]. In addition, modifying nucleocytoplasmic localization may also be a viable approach, as discussed earlier. Selinexor, the first clinically approved nuclear export inhibitor of CRM128, has been shown to cause tumor suppressor proteins to accumulate in the nucleus, thereby reactivating and amplifying their tumor-suppressive function. This leads to selective apoptosis of cancer cells without significantly affecting normal cells[35]. Furthermore, given the characteristic features of MM, such as abnormal plasma cell malignancy and excessive production of antibodies, MM cells (and other blood or solid tumor cells) require proper protein turnover and homeostasis maintenance through PTMs. Abnormal PTMs, such as phosphorylation, acetylation, and ubiquitination, are frequently observed in MM and various types of cancer, which are linked to malignant cell proliferation and drug resistance[2,3,36]. We believe that the discovery of novel therapeutic targets based on abnormal PTMs in different types of cancer and the development of first-class drugs based on these targets are of great value for investigation.

The present study revealed that the direct SUMOylation of p27 by SAE1 contributed to p27 LLPS. LLPS is a newly recognized phenomenon in biological processes, where specific proteins with IDRs and/or nucleic acids can form membrane-less condensates or compartmentalized spaces that frequently exchange materials with their surroundings[37]. The p27 protein belongs to a family of intrinsically unstructured proteins and can be regulated by its expression level, cellular localization, and various PTMs (phosphorylation, ubiquitination, and acetylation)[38]. PTMs have a range of effects, from local stabilization to global order transitions. For example, p27 can shift from acting as a CDK inhibitor to an oncogene when phosphorylated by PI3K effector kinases, as the p27/cJun complex formation and nuclear localization are regulated by p27 phosphorylation[26]. PTMs play a crucial role in driving the assembly or dissociation of the condensates. As a result, the lack of a secondary structure in IDRs makes them particularly susceptible to PTMs[39,40]. SUMOylation is the primary cellular mechanism for modifying lysine residues in IDRs. The IDRs of p27 are enriched in positively charged residues, such as lysine, while the SUMO protein has negative charges, resulting in electrostatic solid interactions. Thus, SUMOylation modification plays a critical role in LLPS, and there is a positive correlation between the SUMOylation of p27 and its LLPS. The SUMOylation of p27 promotes its LLPS, leading to an increased translocation of p27 out of the cell nucleus. Our study also found that p27 could interact with CRM1, a nuclear export receptor, and mutations at the SUMOylation sites of p27 reduced its ability to bind to CRM1. Inhibiting nuclear export with KPT-330 sequesters p27 in the nucleus. Proteins in the condensed state (LLPS) exert stronger biological functions compared to those in the diffused state[41]. Small-molecule therapeutic agents that target nuclear condensates can influence drug activity[42], indicating that suppressing droplet formation or LLPS may be an effective strategy. Our findings demonstrate that colchicine can target SAE1 to disrupt the SUMOylation of p27, exhibiting potential anticancer effects in multiple types of cancer *in vitro* and *in vivo* and positively correlating with the progression-free survival of MM patients.

5. Conclusions

In summary, our study yielded four major results. Firstly, we identified SAE1 as a potential target for colchicine and demonstrated its oncogenic role in MM and other types of human cancer. Secondly, we discovered that SAE1 can enhance the p27 LLPS by SUMOylating the K134 and K190 sites of p27. Thirdly, we demonstrated that SUMOylation-induced nuclear export of p27 can promote MM malignancy, shedding light on the mechanism and functional importance of PTMs in the phase transition of intrinsically disordered proteins. Lastly, through various mouse models, we confirmed that colchicine can prolong survival and delay tumor growth. Our findings have potential implications for using colchicine in clinical treatment for MM, showing promising prospects for large-scale applications.

Acknowledgments

This work was supported by National Natural Science Foundation of China (82341230 to Ye Yang), Basic Research Plan (Natural Science Foundation) in "Climbing" Program of Jiangsu Province (BK20240003 to Ye Yang, China), Science and Technology Development Plan Project of Jiangsu Provincial Administration of Traditional Chinese Medicine (ZD202203 to Chunyan Gu, China), and a project funded by the Priority Academic Program Development of Jiangsu Higher Education Institutions (Traditional Chinese Medicine, Integration of Chinese and Western Medicine) (China). The authors would like to thank participating patients and their families.

Author contributions

Ye Yang and Chunyan Gu conceived the project. Ye Yang, Chunyan Gu , Hongming Huang, and Shiqian Qi supervised the project, reviewed and revised the manuscript. Ling Wang and Jie Min performed the experiments. Ling Wang, Jie Min, and Jinjun Qian analyzed data and drafted the original manuscript. Xiaofang Huang and Shiqian Qi acquired and analyzed the structure biology data. Hongming Huang and Wenfeng Su provided access to the human samples and clinical trial data. Shanliang Sun, Yuhao Cao, and Nianguang Li provided the in vitro binding assay and virtual molecular docking. Mengying Ke collected and visualized high-throughput data using a mass cytometer. Xichao Yu and Xinyu Lv performed animal experiments. Mengjie Guo provided resources and data curation.

Conflicts of interest

The authors declare no financial or commercial conflict of interest.

Appendix A. Supporting information

Supporting information to this article can be found online at https://doi.org/10.1016/j.apsb.2025.02.011.

References

1. van de Donk NWCJ, Pawlyn C, Yong KL. Multiple myeloma. *Lancet* 2021;**397**:410−27.
2. Wirth M, Schick M, Keller U, Kronke J. Ubiquitination and ubiquitin-like modifications in multiple myeloma: biology and therapy. *Cancers* 2020;**12**:3764.
3. Zecha J, Bayer FP, Wiechmann S, Woortman J, Berner N, Muller J, et al. Decrypting drug actions and protein modifications by dose- and time-resolved proteomics. *Science* 2023;**380**:93−101.
4. Flotho A, Melchior F. Sumoylation: a regulatory protein modification in health and disease. *Annu Rev Biochem* 2013;**82**:357−85.
5. Kroonen JS, Vertegaal ACO. Targeting SUMO signaling to wrestle cancer. *Trends Cancer* 2021;**7**:496−510.
6. Yang Y, Liang Z, Xia Z, Wang X, Ma Y, Sheng Z, et al. SAE1 promotes human glioma progression through activating AKT SUMOylation-mediated signaling pathways. *Cell Commun Signal* 2019;**17**:82.
7. Ong JR, Bamodu OA, Khang NV, Lin YK, Yeh CT, Lee WH, et al. SUMO-activating enzyme subunit 1 (SAE1) is a promising diagnostic cancer metabolism biomarker of hepatocellular carcinoma. *Cells* 2021;**10**:178.
8. Driscoll JJ, Pelluru D, Lefkimmiatis K, Fulciniti M, Prabhala RH, Greipp PR, et al. The sumoylation pathway is dysregulated in multiple myeloma and is associated with adverse patient outcome. *Blood* 2010; **115**:2827−34.
9. Lightcap ES, Yu PF, Grossman S, Song KL, Khattar M, Xega K, et al. A small-molecule SUMOylation inhibitor activates antitumor immune responses and potentiates immune therapies in preclinical models. *Sci Transl Med* 2021;**13**:eaba7791.
10. Newman DJ, Cragg GM. Natural products as sources of new drugs over the nearly four decades from 01/1981 to 09/2019. *J Nat Prod* 2020;**83**:770−803.
11. Soignet SL, Frankel SR, Douer D, Tallman MS, Kantarjian H, Calleja E, et al. United States multicenter study of arsenic trioxide in relapsed acute promyelocytic leukemia. *J Clin Oncol* 2001;**19**:3852−60.
12. Zhang TD, Chen GQ, Wang ZG, Wang ZY, Chen SJ, Chen Z. Arsenic trioxide, a therapeutic agent for APL. *Oncogene* 2001;**20**:7146−53.
13. Tang C, Ke MY, Yu XC, Sun SL, Luo X, Liu X, et al. GART functions as a novel methyltransferase in the RUVBL1/β-catenin signaling pathway to promote tumor stemness in colorectal cancer. *Adv Sci* 2023;**10**:e2301264.
14. Gu CY, Wang YJ, Zhang LL, Qiao L, Sun SL, Shao MM, et al. AHSA1 is a promising therapeutic target for cellular proliferation and proteasome inhibitor resistance in multiple myeloma. *J Exp Clin Canc Res* 2022;**41**:11.
15. Cocco G, Chu DCC, Pandolfi S. Colchicine in clinical medicine. A guide for internists. *Eur J Intern Med* 2010;**21**:503−8.
16. Bhattacharya S, Das A, Datta S, Ganguli A, Chakrabarti G. Colchicine induces autophagy and senescence in lung cancer cells at clinically admissible concentration: potential use of colchicine in combination with autophagy inhibitor in cancer therapy. *Tumor Biol* 2016;**37**:10653−64.
17. Jyo T, Endoh H. Clinical experience with Colcemid in true polycythemia and chronic myelogenic leukemia. *Naika Hokan* 1961;**8**:607−15.
18. Broyl A, Hose D, Lokhorst H, de Knegt Y, Peeters J, Jauch A, et al. Gene expression profiling for molecular classification of multiple myeloma in newly diagnosed patients. *Blood* 2010;**116**:2543−53.
19. Olsen SK, Capili AD, Lu XQ, Tan DS, Lima CD. Active site remodelling accompanies thioester bond formation in the SUMO E1. *Nature* 2010;**463**:906−12.
20. Halgren T. New method for fast and accurate binding-site identification and analysis. *Chem Biol Drug Des* 2007;**69**:146−8.
21. Halgren TA. Identifying and characterizing binding sites and assessing druggability. *J Chem Inf Model* 2009;**49**:377−89.
22. Friesner RA, Banks JL, Murphy RB, Halgren TA, Klicic JJ, Mainz DT, et al. Glide: a new approach for rapid, accurate docking and scoring. 1. Method and assessment of docking accuracy. *J Med Chem* 2004;**47**:1739−49.
23. Tang XZ, Guo MJ, Ding PG, Deng ZD, Ke MY, Yuan YX, et al. BUB1B and circBUB1B_544aa aggravate multiple myeloma malignancy through evoking chromosomal instability. *Signal Transduct Tar* 2021;**6**:361.
24. Rutsch S, Neppalli VT, Shin DM, DuBois W, Morse HC, Goldschmidt H, et al. IL-6 and MYC collaborate in plasma cell tumor formation in mice. *Blood* 2010;**115**:1746−54.
25. Zhou H, Lei M, Wang W, Guo MJ, Wang J, Zhang HY, et al. *In vitro* and *in vivo* efficacy of the novel oral proteasome inhibitor NNU546 in multiple myeloma. *Aging* 2020;**12**:22949−74.
26. Razavipour SF, Harikumar KB, Slingerland JM. p27 as a transcriptional regulator: new roles in development and cancer. *Cancer Res* 2020;**80**:3451−8.
27. Currier AW, Kolb EA, Gorlick RG, Roth ME, Gopalakrishnan V, Sampson VB. p27/Kip1 functions as a tumor suppressor and oncoprotein in osteosarcoma. *Sci Rep* 2019;**9**:6161.
28. Coqueret O. New roles for p21 and p27 cell-cycle inhibitors: a function for each cell compartment?. *Trends Cell Biol* 2003;**13**:65−70.
29. Chu IM, Hengst L, Slingerland JM. The Cdk inhibitor p27 in human cancer: prognostic potential and relevance to anticancer therapy. *Nat Rev Cancer* 2008;**8**:253−67.
30. Das RK, Huang YQ, Phillips AH, Kriwacki RW, Pappu RV. Cryptic sequence features within the disordered protein p27 regulate cell cycle signaling. *Proc Natl Acad Sci U S A* 2016;**113**:5616−21.
31. Fung HY, Chook YM. Atomic basis of CRM1-cargo recognition, release and inhibition. *Semin Cancer Biol* 2014;**27**:52−61.
32. Cowan AJ, Green DJ, Kwok M, Lee S, Coffey DG, Holmberg LA, et al. Diagnosis and management of multiple myeloma: a review. *JAMA* 2022;**327**:464−77.
33. Zhao ZJ, Chen Y, Francisco NM, Zhang YQ, Wu MH. The application of CAR-T cell therapy in hematological malignancies: advantages and challenges. *Acta Pharm Sin B* 2018;**8**:539−51.
34. Langston SP, Grossman S, England D, Afroze R, Bence N, Bowman D, et al. Discovery of TAK-981, a first-in-class inhibitor of SUMO-activating enzyme for the treatment of cancer. *J Med Chem* 2021;**64**:2501−20.
35. Benkova K, Mihalyova J, Hajek R, Jelinek T. Selinexor, selective inhibitor of nuclear export: unselective bullet for blood cancers. *Blood Rev* 2021;**46**:100758.
36. Lu K, Zhang M, Qin HY, Shen SY, Song HQ, Jiang H, et al. Disruption of cyclin D1 degradation leads to the development of mantle cell lymphoma. *Acta Pharm Sin B* 2024;**14**:2977−91.
37. Brangwynne CP, Eckmann CR, Courson DS, Rybarska A, Hoege C, Gharakhani J, et al. Germline P granules are liquid droplets that localize by controlled dissolution/condensation. *Science* 2009;**324**:1729−32.
38. Bencivenga D, Caldarelli I, Stampone E, Mancini FP, Balestrieri ML, Della Ragione F, et al. p27 and human cancers: a reappraisal of a still enigmatic protein. *Cancer Lett* 2017;**403**:354−65.
39. Dyson HJ. Expanding the proteome: disordered and alternatively folded proteins. *Q Rev Biophys* 2011;**44**:467−518.
40. Bah A, Forman-Kay JD. Modulation of intrinsically disordered protein function by post-translational modifications. *J Biol Chem* 2016;**291**: 6696−705.
41. Strom AR, Brangwynne CP. The liquid nucleome—phase transitions in the nucleus at a glance. *J Cel Sci* 2019;**132**:jcs235093.
42. Klein IA, Boija A, Afeyan LK, Hawken SW, Fan M, Dall'Agnese A, et al. Partitioning of cancer therapeutics in nuclear condensates. *Science* 2020;**368**:1386−92.